Research Article | Vol. 27, No. 14 | 8 Jul 2019 | OPTICS EXPRESS 19426
Optics EXPRESS

Silicon photonic switch-based optical equalization for mitigating pulsewidth distortion

YU-HAN HUNG,[1,2] QIXIANG CHENG,[1,*] MADELEINE GLICK,[1] MEISAM BADAHORI,[1] LIANG YUAN DAI,[1] AND KEREN BERGMAN[1]

[1]*Department of Electrical Engineering, Columbia University, New York, NY 10027, USA*
[2]*yh3128@columbia.edu*
**qc2228@columbia.edu*

Abstract: Optical transmitters typically require electrical pre-amplification using driver amplifiers to optimize the optical modulation depth. To enhance the detection sensitivity and optimize the overall link budget, equalization is required to compensate for undesired signal distortion induced by the transmitter. In this paper, we propose and demonstrate a novel optical equalization scheme using a silicon photonic micro-ring resonator (MRR)-based switching circuit for mitigating driver-amplifier-induced pulsewidth distortion. The switching circuit simultaneously functions as a spatial optical switch as well as a two-stage optical bandpass filter for optical equalization. The experimental results indicate a 4.5-dB detection sensitivity enhancement at a data rate of 12.5 Gbits/s. The proposed approach is robust to different levels of pulsewidth distortion without additional signal processing, and has possibilities to support higher data rates by adjusting the MRR parameters.

1. Introduction

With the growing diversity of communication intensive big data applications, including cloud-based services and high-performance data analytics, current datacenter architectures are increasingly challenged by these workloads. Disaggregated network architectures with photonic switched interconnects, sharing computing and/or memory resources among servers via a photonic switched interconnect, have been proposed as a solution to this challenge [1–4]. Silicon photonic (SiP) switches are emerging as prime candidates for optical switching in data center interconnection networks since SiP switch fabrics combine the advantages of supporting high bandwidth density and low-latency switching, while occupying a small footprint and operating with low power consumption [1,5,6].

To efficiently transmit data in datacenters, Non-return-to-zero (NRZ) signaling for intensity modulation and direct detection (IMDD) systems is currently preferred due to the primary metrics of cost and power consumption [7,8].Optical transmitters in such IMDD systems typically employ electrical pre-amplification using driver amplifiers to optimize optical modulation depth through optical intensity modulation [9–12]. Due to the nonlinearity that arises from offset voltages in driver amplifiers, pulsewidth distortion induced by driver amplifiers leads to unequal periods of logic one-level and zero-level and consequently reduces the overall link detection sensitivity [13]. As reported in [14], the offset voltages can be compensated using electronic circuits, which adds power consumption and complexity to the system. In this paper, we demonstrate a technique that can be utilized to equalize this transmitted pulsewidth distortion in photonic circuits containing SiP micro-ring resonator (MRR)-based switching fabrics. This approach is not only robust to different levels of pulsewidth distortion without additional signal processing or computing, but also potentially capable of supporting higher data rates by adjusting MRR parameters. Moreover, since the device primarily serves the function of optical switching, our approach efficiently eliminates

#365493 https://doi.org/10.1364/OE.27.019426
Journal © 2019 Received 18 Apr 2019; revised 25 May 2019; accepted 27 May 2019; published 26 Jun 2019

Optics EXPRESS

the need for the additional optical equalization mitigating the transmitter impairment in photonic integrated circuits containing MRR-based switches.

2. Operation principle

The operation principle is depicted in Fig. 1. Electrical data $E(t)$ generated from a pattern generator is given by

$$E(t) = |A(t)| e^{i\angle P(t)} \tag{1}$$

The electrical data is distorted by the driver amplifiers working in its nonlinear region through gain saturation. The saturated driver amplifier therefore generates undesirable harmonic distortion components for the electrical data. The distorted electrical data $D(t)$ thus includes amplitude distortion $g(|A(t)|)$and phase distortion $f(|A(t)|)$. The distorted electrical data $D(t)$ can be given by

$$D(t) = g(|A(t)|)e^{i(\angle P(t)+f(|A(t)|))} \tag{2}$$

An external modulator then superimposes the distorted electrical data onto the optical carrier generated from the tunable laser diode, forming the input optical signals, as shown in Fig. 1. The input optical signals $S_{in}(t)$ can be described by

$$S_{in}(t) = (1 + D(t))(m\cos(2\pi f_c t)) \tag{3}$$

where $m$is amplitude-modulation index, and f_c is optical carrier frequency. One sees, the nonlinear distortion components appear around the null points on both sides of the optical carrier. The proposed switching circuit functions as a symmetric optical filter, thereby suppressing the signal distortion [15]. This can be described by

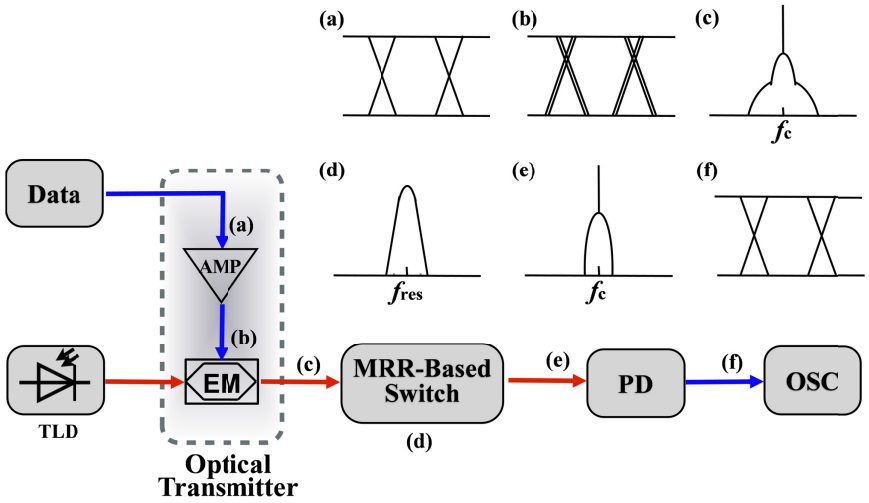

Fig. 1. Operation principle.(a) eye-diagram of electrical data; (b) eye-diagram of distorted electrical data; (c) input optical signals; (d) frequency response of the MRR-Based Switch; (e) output optical signals; (f) eye-diagram of output optical signals; AMP, driver amplifier; TLD, tunable laser diode; EM external modulator; PD photodiode; OSC, oscilloscope.

$$F(f) \approx \frac{F_0}{1 + (\frac{2}{\Delta f_{3dB}}(f - f_{res}))^2} \tag{4}$$

Optics EXPRESS

where $F_0$is the optical attenuation of MRR, $\Delta f_{3dB}$is the 3 dB optical bandwidth, and $f_{res}$is the MRR resonance frequency. To understand how the distortion compensation occurs we note the following: From Eq. (3) and a corresponding Fourier transform $\tilde{S}_{in}(f)$,the output optical signals $\tilde{S}_{out}(f)$ can be described by

$$\tilde{S}_{out}(f) \approx \tilde{S}_{in}(f)F(f)e^{\left(-i\beta''\frac{(2\pi(f-f_c))^2 L}{2}\right)} \tag{5}$$

where $\beta''$is waveguide dispersion parameter, and L is the waveguide length. When the switching circuit performing a symmetric optical filter is at $f_{res} = f_c$, and Δf_{3dB}matches the passband of the input optical signals, the distortion components can be effectively suppressed, resulting in a clearer eye-diagram after photodetection. Note that the excess optical attenuation of MRR can decrease the quality of the eye-diagram after photodetection through reducing the link power budget. An optical power amplifier is required to compensate the optical power attenuation.

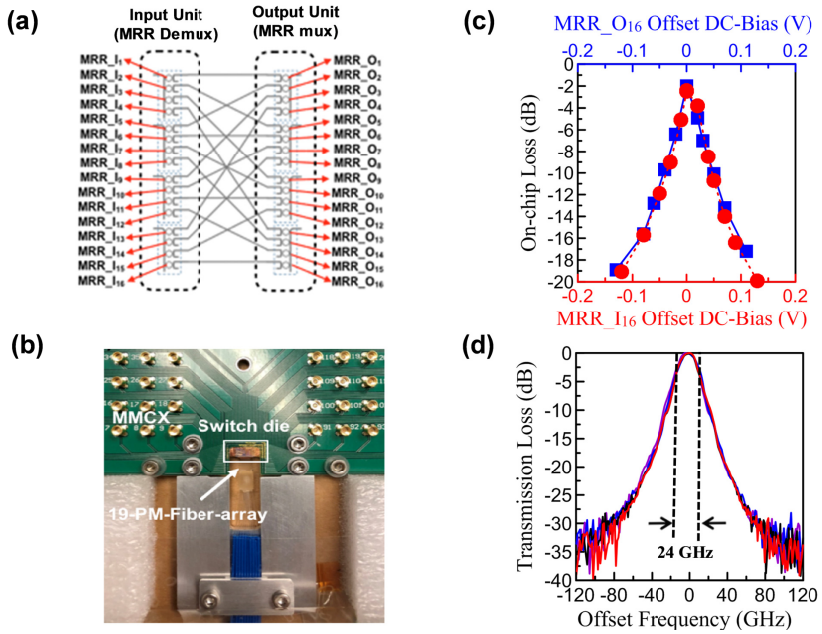

Fig. 2. (a) Schematic of the 4 × 4 MRR-based switch-and-select switching fabric. (b) Photo of the packaged switching circuit. (c) Transmission loss in terms of MRR DC-Bias. Note that the upper x-axis and the lower x-axis are offset to 1.12 Volt and 0.86 Volt, respectively.(d) Normalized transmission spectra of a set of representative paths. Note that the edge coupling loss of the switching circuit is 11 dB [16].

3. Switch device and control

A layout of the SiP MRR-based 4 × 4 switch-and-select switching circuit is shown in Fig. 2(a). The switching circuit is composed of two (input and output) switching units connected by a passive shuffle network [16]. The switching units are designed using 32 micro-heater-integrated MRR elements forming four 1 × 4 spatial multiplexers and four 4 × 1 spatial de-multiplexers in a bus structure. The switching circuit was taped out using standard PDK elements through the AIM Photonics multi-project wafer (MPW) run and has a compact footprint of 1.5 × 2.4 mm^2 with 32 control electrodes and 2 common grounds. More information can be found in [16]. A microscope photo of the fabricated chip and the packaged switching circuit is shown in Fig. 2(b).

Optics EXPRESS

To implement a switch-and-select topology in the switching circuit, the selected MRR elements in the input and output unit should be kept on the resonance state [17]. However, since the optical behavior of the MRR is sensitive to thermal effects, temperature conditions of the MRR elements are controlled using integrated micro-heaters with DC-bias control [18–20]. For example, input optical signals at 194.8 THz can pass through the optical path 4-4 of the switching circuit when the MRR_I_{16} and the MRR_O_{16} are DC-biased at 0.86 Volt and 1.12 Volt, respectively, leading to a 2-dB on-chip loss, as shown in Fig. 2(c). Note that the switching circuit is designed to operate critical coupling. When the DC-bias values of the MRR elements are tuned out of the optimal condition, the on-chip loss gradually increases due to the shifted resonance frequencies of the MRR elements [18–20]. Additionally, in the switch-and-select topology, the 1st order crosstalk leakage due to the off-resonance state is effectively canceled through the second add-drop filtering when a channel spacing between the on and off-resonance state is 12 nm, which corresponds to half of free spectral range of the MRR elements [16]. The switching circuit accordingly performs as a two-stage optical filter and exhibits crosstalk suppression of over 50 dB with an on-off extinction ratio of over 25 dB from each of the MRR elements [16]. A 3-dB passband of approximately 24 GHz, which is consistently measured on all the optical paths, with a filtering roll-off slope of 60

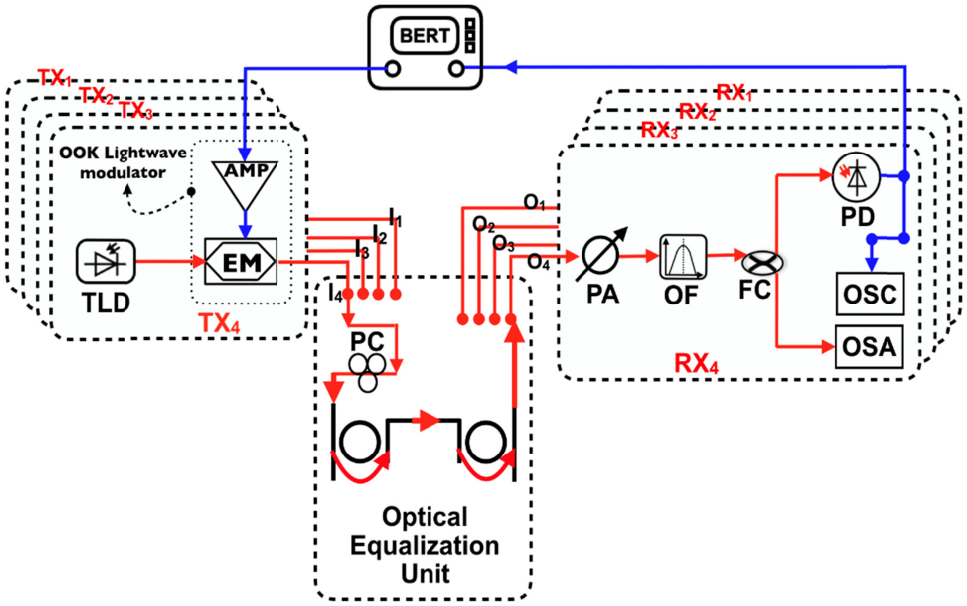

Fig. 3. Schematic of the experimental apparatus. AMP, driver amplifier; TLD, tunable laser diode; EM, external modulator; PC, polarization controller; PA, power adjuster; OF optical filter; FC, fiber coupler, PD, photodiode; OSC, oscilloscope; OSA, optical spectrum analyzer; BERT, bit-error-rate tester.

dB/nm is shown in Fig. 2(d).

4. Experimental setup

The schematic of the experimental apparatus based on the SiP MRR-based 4 × 4 switching circuit is presented in Fig. 3. As will be shown in the following, the switching circuit also functions as the primary optical equalization unit. On the transmitter side (TX), a commercial tunable laser diode generates input optical carriers at 194.8 THz. An on-off keying (OOK) lightwave modulator (Optilab LM-OOK-50R-EL) consists of a driver amplifier and an external intensity modulator. The driver amplifier is used to amplify electrical NRZ signals, which are generated from a pattern generator in a bit error rate tester (Anritsu MP1800), with a pseudorandom binary sequence (PRBS) of 2^{31}-1. The driver amplifier thus outputs the

Optics EXPRESS

electrical NRZ signals with a fixed peak-to-peak voltage (V_{pp}) of 1.3 Volt. The external intensity modulator, where the V_π is 3.5 Volt, operated at its quadrature point superimposes the electrical NRZ signals onto the intensity of the input optical carriers, forming input NRZ-encoded optical signals. Since the switching circuit is a polarization dependent device, a polarization controller is used to TE-polarize the input NRZ-encoded optical signals prior to the switching circuit for reducing additional insertion loss. To guide the input NRZ-encoded optical signals to pass through a selected optical path of the switching circuit, a center frequency of the path band is adjusted to the input optical carrier frequency under a DC-bias control. On the receiver side (RX), a power adjuster consisting of an optical amplifier and an optical attenuator is utilized to compensate the optical power loss through the switching circuit. Note that the maximum noise figure of the optical amplifier is 6 dB. Additional amplified spontaneous emission noise, which is induced by the optical amplifier, is suppressed using an optical filter (BVF-200) with a bandwidth of 50 GHz. The output NRZ-encoded optical signals are displayed on an optical spectrum analyzer (BOSA 400), and a sampling oscilloscope following a 43-Gbits/s photodiode (Finisar XPR2022A). Finally, bit-error ratio (BER) analysis is performed with the error tester in the BERT.

5. Results and analysis

5.1 Driver-amplifier-induced distortion

To realize the proposed optical equalization, we consider the signal distortion induced by a driver amplifier in the OOK lightwave modulator. We first consider the situation of the driver amplifier in its linear region. Electrical NRZ signals at a data rate of 12.5 Gbits/s, with a power spectrum following a $(\sin^2 x)/x^2$ pattern [21],are amplified using the driver amplifier, and then drives an external intensity modulator generating the input NRZ-encoded optical signals, as shown in Fig. 4(a). As can be seen in Fig. 4(b), the modulation signals are symmetric in intensity and are 35-dB weaker than the input optical carriers. After photodetection, a clear eye-diagram with an input eye-crossing-percentage (ECP) of 50% is obtained, as shown in Fig. 4(d). The ECP is calculated as follows [21]:

$$\mathrm{ECP} = \frac{\text{Crossing Level - Zero Level}}{\text{One Level - Zero Level}} \times 100\% \tag{6}$$

We next consider the situation of the driver amplifier in its nonlinear region. Since the driver amplifier distorts the electrical NRZ signals through offset voltages in the driver amplifier [13], the resulting input NRZ-encoded optical signals exhibit nonlinear distortion components around the null points at ± 12.5 GHz. As shown in Fig. 4(e), the eye-diagram exhibits an extension of the one-level periods and a reduction of the zero-level periods, resulting in an input ECP of 73%.

5.2 Optical equalization using a MRR-based switch

By taking advantage of the symmetric optical filtering nature of MRR elements, the proposed switching circuit is used to function as an optical equalization unit. The optical path 4-4 of the switching circuit is described here as an example. First, to guide the input NRZ-encoded optical signals, as shown in Fig. 4(b), passing through the optical path 4-4 of the switching circuit, the MRR_I_{16} and the MRR_O_{16} are DC-biased at 0.86 Volt and 1.12 Volt, respectively. An optical spectrum of the output NRZ-encoded optical signals at the fourth drop port (O_4) of the switch is shown in Fig. 4(c). As can be seen, since the switching circuit performs a two-stage optical bandpass filter, the nonlinear distortion components are effectively suppressed by at least 5 dB while the other optical components between ± 12.5 GHz are preserved. As shown in Fig. 4(f), a clearer eye-diagram with an output ECP of around 59% is thus observed.

Optics EXPRESS

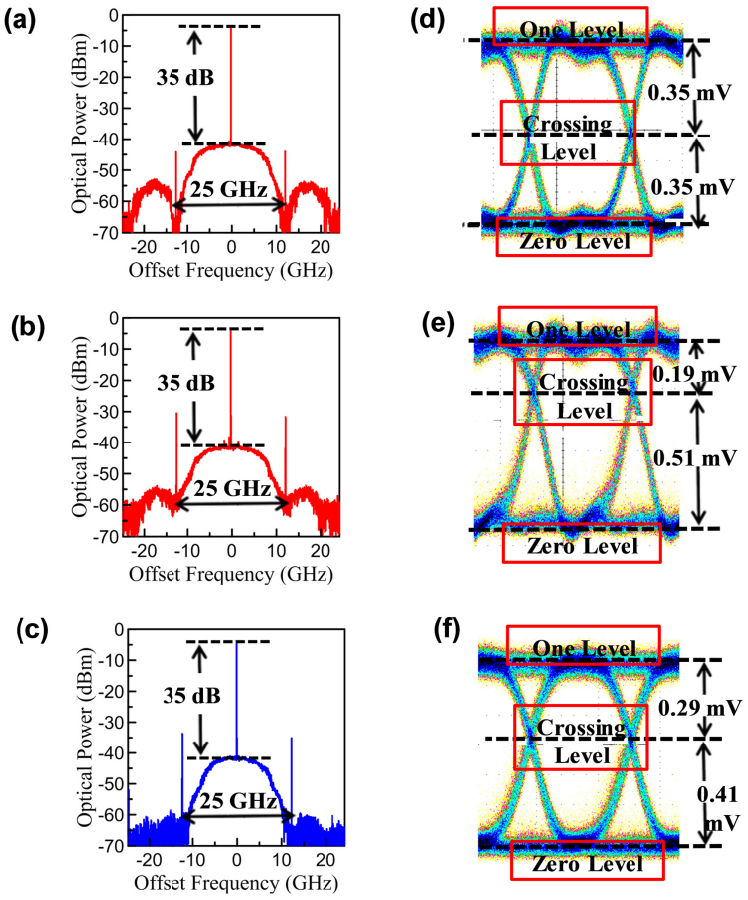

Fig. 4. Optical spectra of input NRZ-encoded optical signals with 50% ECP (a), 73% ECP (b), and output NRZ-encoded optical signals (c), respectively. The x-axes are offset to the input optical carrier frequency. When measuring the optical spectra, a resolution of 10 MHz is used. (d), (e), (f) Eye-diagrams for (a), (b), and (c), respectively.

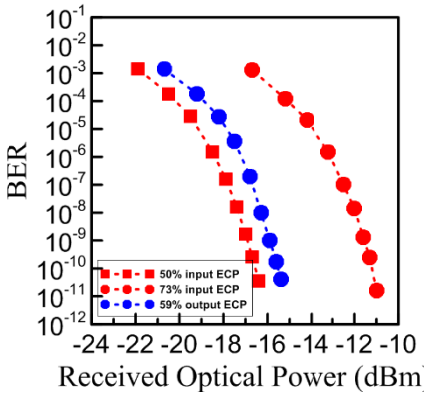

Fig. 5. BER in terms of received optical power. Red circles and red squares, input NRZ-encoded optical signals with 73% ECP and 50%, respectively; blue circles, output NRZ-encoded optical signals with 59% ECP.

Optics EXPRESS

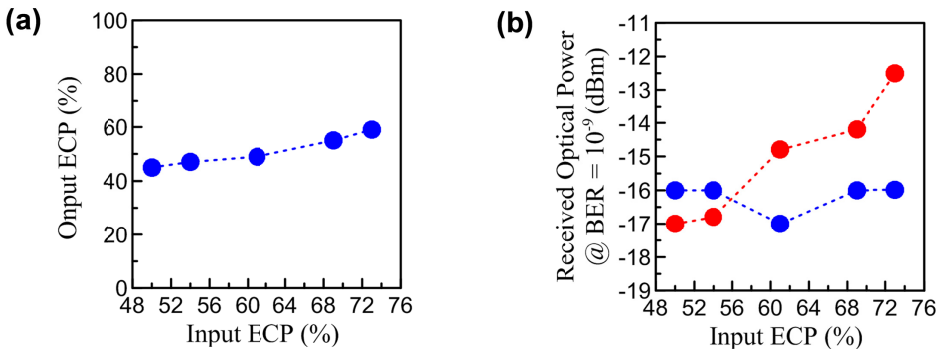

Fig. 6. (a) Output ECP in terms of input ECP. (b) Received optical power in photodiode in terms of input ECP. The red circles and blue circles are input NRZ-encoded optical signals and output NRZ-encoded optical signals, respectively.

Figure 5 presents a BER analysis of the signal quality. First, the driver-amplifier-induced distortion leads to a considerable 5.5-dB power penalty (red squares and red circles). The signal distortion is suppressed due to the optical equalization. As a result, a BER better than 10^{-9} is achieved with a power penalty of approximately –4.5 dB (red circles and blue circles).

To study the quality of the proposed optical equalization's robustness to different levels of distortion, the driver amplifier is operated with a range of input ECP from 50% to 73%. Under such variation, the output NRZ-encoded optical signals show ECPs of approximately 50%, as shown in Fig. 6(a).Accordingly, as shown in Fig. 6(b), detecting the output NRZ-encoded optical signals exhibits stable received optical power in the photodiode at BER = 10^{-9}.The same investigation for the input NRZ-encoded optical signals without the optical equalization is also studied. As shown in Fig. 6(b), the received optical power at BER = 10^{-9} increases with the increasing input ECP. This result agrees with the fact that the ECP higher than 50% leads to poorer detection sensitivity when the optical equalization is not applied [13,22].

To further evaluate the performance of the proposed approach, power penalty at BER = 10^{-9} regarding data rate of input NRZ-encoded optical signals is studied. As shown in Fig. 7, power penalty reaches its minimum value at around 12.5 Gbits/s, and increases monotonically when the data rate deviates from 12.5 Gbits/s. Such a dependence results from the fact of the 3-dBpassing bandwidth of the proposed switching circuit, as presented in Fig. 2(d). For the data rate lower than 12.5 Gbits/s, BER behavior of the output NRZ-encoded optical signals are close to that of the input signals, leading to the power penalty of near 0 dB, since a bandwidth of the input NRZ-encoded optical signals is lower than the 3-dB passing bandwidth of the switching circuit. For data rates higher than 12.5 Gbits/s, since the limited 3-dB passing bandwidth of the switching circuit leads to intersymbol interference, the power penalty accordingly increases with the data rate.

Optics EXPRESS

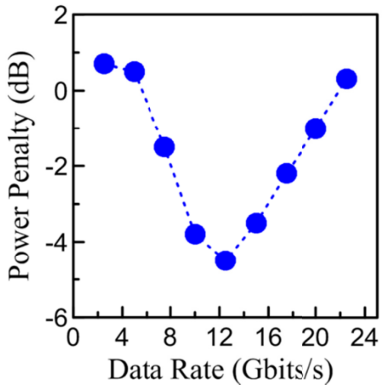

Fig. 7. Power penalty in terms of data rate. Note that the input ECP is kept at 73%.

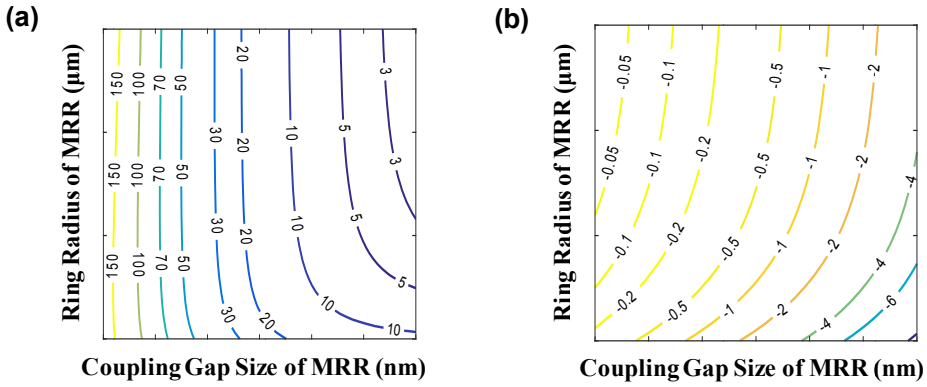

Fig. 8. (a) Mappings of the MRR 3-dB passband (a) and MRR optical power loss (b) as a function of coupling gap size of MRR and ring radius of MRR. Each contour line in (a) indicates a constant 3-dB passband, as marked, in GHz. Each contour line in (b) indicates a constant optical power loss, as marked, in dB.

5.3 Adjusting the passband of MRR switch fabrics

To achieve the optimal optical equalization at different data rates, the 3-dB passband of MRR switch circuit should be adjusted to match the system requirement. In this section, we explore the design space of individual microring switching cells, specially their 3dB optical bandwidth, with foundry-validated data. A set of key foundry related parameters on the bending loss of the ring resonators as a function of radius were first collected through AIM MPW runs. The method that is used to establish the compact model is described in [15]. Detailed bandwidth contours of the add-drop microring unit as a function of its geometrical parameters, i.e. ring radius and ring-bus gap, are plotted in Fig. 8(a). The contour lines not only indicate that the 3-dB passband of MRR decreases with a coupling gap size of MRR, but also exhibit a widely tunable 3-dB passband of over 150 GHz, which indicates the feasibility of suppoting data rates up to 75 Gbits/s, offering a great design flexibility.In addition, as shown in Fig. 8(b), the optical power loss is from 0.05 dB to 0.5 dB when the 3-dB passband is higher than 10 GHz. An optimization of the optical power loss is also feasible by selecting an appropriate combination of coupling gap size and ring radius. The low power loss can be further compensated by using optical power amplifiers while maintaining the similar behavior of BER. In this study we restrict the ring-bus gap to be larger than 100 nm as the fabrication becomes difficult at smaller gaps. It should, however, be noted that a structure based on cascaded MRRs can potentially be used for tuning the 3-dB passbands [23], at the expense of increased loss and control complexity.

Optics EXPRESS

6. Conclusions

This study demonstrates driver-amplifier-induced pulsewidth distortion equalization for photonic switched interconnects using a SiP MRR-based switching circuit. The switching circuit is shown to function as both a spatial optical switch and an optical equalization unit. A 4.5-dB detection sensitivity enhancement is obtained at a data rate of 12.5 Gbits/s. The proposed approach is robust to different levels of pulsewidth distortion, and potentially capable of supporting higher data rates by adjusting MRR parameters. Our approach thus eliminates additional electronic signal processing and the related power consumption to overcome this transmitter impairment. As the underlying mechanism relies on optical filtering suppressing nonlinear distortion components close to the filtering edge of the switching circuit, it can also apply to MRR-based switches with different architectures, such as Hitless router [24], Crossbar [25] and Benes [26]. It should be noted that cascading multiple MRRs, which can form a multi-stage switch, may induce higher optical power loss, bandwidth narrow-down effect, and group delay effect [27,28]. Moreover, by using one filtering edge for asymmetric optical filtering, this technique may be applied to compensate the chirp effect, induced by optical intensity modulation [29,30].

Acknowledgement

This work is based on research sponsored by Air Force Research Laboratory under agreement number FA8650-15-2-5220. The U.S. Government is authorized to reproduce and distribute reprints for Governmental purposes notwithstanding any copyright notation thereon. The views and conclusions contained herein are those of the authors and should not be interpreted as necessarily representing the official policies or endorsements, either expressed or implied, of Air Force Research Laboratory or the U.S. Government. This work is also partially supported by the ARPA-E ENLITENED program (DEAR00000843).

Funding

Air Force Research Laboratory (AFRL) (FA8650- 15-2-5220); Advanced Research Projects Agency—Energy (ARPA-E) (ENLITENED); U.S. Department of Energy (DOE) (DE-AR0000843).

References

1. Q. Cheng, M. Bahadori, M. Glick, S. Rumley, and K. Bergman, "Recent advances in optical technologies for data centers: a review," Optica **5**(11), 1354–1370 (2018).
2. B. Abali, R. J. Eickemeyer, H. Franke, C. S. Li, and M. A. Taubenblatt, "Disaggregated and optically interconnected memory: when will it be cost effective?" arXiv:1503.01416 (2015).
3. Y. Yan, G. M. Saridis, Y. Shu, B. R. Rofoee, S. Yan, M. Arslan, T. Bradley, N. V. Wheeler, N. H. L. Wong, F. Poletti, M. N. Petrovich, D. J. Richardson, S. Poole, G. Zervas, and D. Simeonidou, "All-optical programmable disaggregated data center network realized by FPGA-based switch and interface card," J. Lightwave Technol. **34**(8), 1925–1932 (2016).
4. Q. Cheng, S. Rumley, M. Bahadori, and K. Bergman, "Photonic switching in high performance datacenters [Invited]," Opt. Express **26**(12), 16022–16043 (2018).
5. D. Blumenthal, K. Y. Chen, J. Ma, R. J. Feuerstein, and J. R. Sauer, "Demonstration of a deflection routing 2×2 photonic switch for computer interconnects," IEEE Photonics Technol. Lett. **4**(2), 169–173 (1992).
6. K. L. Deng, R. J. Runser, P. Toliver, I. Glesk, and P. R. Prucnal, "A highly-scalable, rapidly-reconfigurable, multicasting-capable, 100 Gb/s photonic switched interconnect based upon OTDM technology," J. Lightwave Technol. **18**(12), 1892–1904 (2000).
7. J. L. Wei, J. D. Ingham, D. G. Cunningham, R. V. Penty, and I. H. White, "Performance and power dissipation comparisons between 28 Gb/s NRZ, PAM, CAP and Optical OFDM systems for data communication applications," J. Lightwave Technol. **30**(20), 3273–3280 (2012).
8. J. L. Wei, Q. Cheng, R. V. Penty, I. H. White, and D. G. Cunningham, "400 Gigabit Ethernet using advanced modulation formats: performance, complexity, and power dissipation," IEEE Commun. Mag. **53**(2), 182–189 (2015).
9. N. Eiselt, J. Wei, H. Griesser, A. Dochhan, M. H. Eiselt, J. P. Elbers, J. J. V. Olmos, and I. T. Monroy, "Evaluation of Real-Time 8 × 56.25 Gb/s (400G) PAM-4 for Inter-Data Center Application Over 80 km of SSMF at 1550 nm," J. Lightwave Technol. **35**(4), 955–962 (2017).

Optics EXPRESS

10. R. Rodes, M. Mueller, B. Li, J. Estaran, J. Jensen, T. Gruendl, M. Ortsiefer, C. Neumeyr, J. Rosskopf, K. Larsen, M. Amann, and I. Monroy, "High-speed 1550 nm VCSEL data transmission link employing 25 GBd 4-PAM modulation and hard decision forward error correction," J. Lightwave Technol. **31**(4), 689–695 (2013).
11. X. Zheng, D. Patil, J. Lexau, F. Liu, G. Li, H. Thacker, Y. Luo, I. Shubin, J. Li, J. Yao, P. Dong, D. Feng, M. Asghari, T. Pinguet, A. Mekis, P. Amberg, M. Dayringer, J. Gainsley, H. F. Moghadam, E. Alon, K. Raj, R. Ho, J. E. Cunningham, and A. V. Krishnamoorthy, "Ultra-efficient 10 Gb/s hybrid integrated silicon photonic transmitter and receiver," Opt. Express **19**(6), 5172–5186 (2011).
12. H. Ramon, M. Vanhoecke, J. Verbist, W. Soenen, P. DeHeyn, Y. Ban, M. Pantouvaki, J. VanCampenhout, P. Ossieur, X. Yin, and J. Bauwelinck, "Low-power 56Gb/s NRZ microring modulator driver in 28nm FDSOI CMOS," IEEE Photonics Technol. Lett. **30**(5), 467–470 (2018).
13. B. Razavi, *Design of Integrated Circuits for Optical Communications* (McGraw-Hill, 2003), Chap.10.
14. A. R. Mohamed, M. F. Ibrahim, and F. Farag, "Input offset cancellation trimming technique for operational amplifiers," in Proceedings of the Saudi International Conference on Electronics, Communications, and Photonics (SIECPC, 2013), pp. 1–5.
15. M. Bahadori, M. Nikdast, S. Rumley, L. Y. Dai, N. Janosik, T. Van Vaerenbergh, A. Gazman, Q. Cheng, R. Polster, and K. Bergman, "Design space exploration of microring resonators in silicon photonic interconnects: impact of the ring curvature," J. Lightwave Technol. **36**(13), 2767–2782 (2018).
16. Q. Cheng, L. Y. Dai, N. C. Abrams, Y. H. Hung, P. E. Morrissey, M. Glick, P. O'Brien, and K. Bergman, "Ultralow-crosstalk, strictly non-blocking microring-based optical switch," Photon. Res. **7**(2), 155–161 (2019).
17. W. Bogaerts, P. De Heyn, T. Van Vaerenbergh, K. De Vos, S. K. Selvaraja, T. Claes, P. Dumon, P. Bienstman, D. Van Thourhout, and R. Baets, "Silicon microring resonators," Laser Photonics Rev. **6**(1), 47–73 (2012).
18. K. Padmaraju, J. Chan, L. Chen, M. Lipson, and K. Bergman, "Thermal stabilization of a microring modulator using feedback control," Opt. Express **20**(27), 27999–28008 (2012).
19. H. Jayatilleka, K. Murray, M. Á. Guillén-Torres, M. Caverley, R. Hu, N. A. F. Jaeger, L. Chrostowski, and S. Shekhar, "Wavelength tuning and stabilization of microring-based filters using silicon in-resonator photoconductive heaters," Opt. Express **23**(19), 25084–25097 (2015).
20. M. Bahadori, A. Gazman, N. Janosik, S. Rumley, Z. Zhu, R. Polster, Q. Cheng, and K. Bergman, "Thermal Rectification of Integrated Microheaters for Microring Resonators in Silicon Photonics Platform," J. Lightwave Technol. **36**(3), 773–788 (2018).
21. R. N. Mutagi, "Pseudo noise sequences for engineers," Electron. Commun. Eng. **8**(2), 79–87 (1996).
22. J. Ruzbarsky, J. Turan, and L. Ovsenik, "Effects act on transmitted signal in a fully optical fiber WDM systems," in Proceedings of the IEEE 13th International Scientific Conference onInformatics (INFORMATICS, 2015), pp. 217–221.
23. T. Dai, A. Shen, G. Wang, Y. Wang, Y. Li, X. Jiang, and J. Yang, "Bandwidth and wavelength tunable optical passband filter based on silicon multiple microring resonators," Opt. Lett. **41**(20), 4807–4810 (2016).
24. N. Sherwood-Droz, H. Wang, L. Chen, B. G. Lee, A. Biberman, K. Bergman, and M. Lipson, "Optical 4x4 hitless slicon router for optical networks-on-chip (NoC)," Opt. Express **16**(20), 15915–15922 (2008).
25. A. S. P. Khope, A. M. Netherton, T. Hirokawa, N. Volet, E. J. Stanton, C. Schow, R. Helkey, A. A. M. Saleh, J. E. Bowers, and R. C. Alferness, "Elastic WDM optoelectronic crossbar switch with on-chip wavelength control," in Proceedings of Advanced Photonics Congress (IPR, Networks, NOMA, PS, Sensors, SPPCom, 2017), PTh1D.3.
26. Q. Zhu, *et al*., "Automated wavelength alignment in a 4 × 4 silicon thermooptic switch based on dual-ring resonators," IEEE Photonics J. **10**, 1–12 (2018).
27. J. L. Wei, C. Sánchez, E. Hugues-Salas, P. S. Spencer, and J. M. Tang, "Wavelength-offset filtering in optical OFDM IMDD systems using directly modulated DFB lasers," J. Lightwave Technol. **29**(18), 2861–2870 (2011).
28. Q. Cheng, M. Bahadori, Y. H. Hung, Y. Huang, N. Abrams, and K. Bergman, "Scalable microring-based silicon clos switchfabric with switch-and-select stages," IEEE J. Sel. Top. Quantum Electron. **25**(5), 3600111 (2019).
29. P. A. Morton, G. E. Shtengel, L. D. Tzeng, R. D. Yadvish, T. Tanbun-Ek, and R. A. Logan, "38.5 km error free transmission at 10 Gbit/s in standard fiber using a low chirp, spectrally filtered, directly modulated 1.55 um DFB laser," Electron. Lett. **33**(4), 310–311 (1997).
30. L. S. Yan, Y. Wang, B. Zhang, C. Yu, J. McGeehan, L. Paraschis, and A. E. Willner, "Reach extension in 10-Gb/s directly modulated transmission systems using asymmetric and narrowband optical filtering," Opt. Express **13**(13), 5106–5115 (2005).